6-29-2017

The solidification of Al–Pd–Mn studied by high-energy X-ray diffraction from electrostatically levitated samples

Dante G. Quirinale
Iowa State University

Andreas Kreyssig
Iowa State University and Ames Laboratory, kreyssig@ameslab.gov

Scott M. Saunders
Iowa State University, smsaund@iastate.edu

Daniel Messina
Iowa State University

Warren E. Straszheim
Ames Laboratory, wesaia@iastate.edu

See next page for additional authors

The solidification of Al–Pd–Mn studied by high-energy X-ray diffraction from electrostatically levitated samples

Abstract

We report on the results of a high-energy x-ray diffraction study of Al–Pd–Mn to investigate the solidification products obtained during free-cooling using an electrostatic levitation furnace. The primary solidification product from the melt is *i*-Al–Pd–Mn which coexists with a significant remaining liquid component. As the sample cools further, we find that the solidification pathway is consistent with the liquidus projection and pseudo-binary cut through the ternary phase diagram reported previously. At ambient temperature we have identified the major phase to be the ξ'-phase orthorhombic approximant, along with minor phases identified as Al and, most likely, the R-phase orthorhombic approximant. We have also observed a distinct prepeak in the liquid at high temperature, signifying the presence of extended atomic order. Interestingly, this prepeak was not observed in previous neutron diffraction measurements on the Al–Pd–Mn system. No undercooling was observed preceding the solidification of the *i*-Al–Pd–Mn phase from the melt which may signal the close similarity of the short-range order in the solid and liquid. However, this can not be clearly determined because of the potential for heterogenous nucleation associated with the presence of an Al2O3 impurity at the surface of the sample.

Keywords

electrostatic levitation, high-energy x-ray diffraction, icosahedral phase, phase determination, quasicrystals

Disciplines

Physics

Comments

This article is published as Quirinale, Dante G., Andreas Kreyssig, Scott Saunders, Daniel Messina, Warren E. Straszheim, Paul C. Canfield, Matthew J. Kramer, and Alan I. Goldman. "The solidification of Al–Pd–Mn studied by high-energy X-ray diffraction from electrostatically levitated samples." *Zeitschrift für Kristallographie-Crystalline Materials* 232, no. 7-9 (2017): 619-627. DOI: 10.1515/zkri-2016-2037. Posted with permission.

Authors

Dante G. Quirinale, Andreas Kreyssig, Scott M. Saunders, Daniel Messina, Warren E. Straszheim, Paul C. Canfield, Matthew J. Kramer, and Alan I. Goldman

Dante G. Quirinale, Andreas Kreyssig, Scott Saunders, Daniel Messina, Warren E. Straszheim, Paul C. Canfield, Matthew J. Kramer and Alan I. Goldman*

The solidification of Al–Pd–Mn studied by high-energy X-ray diffraction from electrostatically levitated samples

DOI 10.1515/zkri-2016-2037
Received December 16, 2016; accepted April 27, 2017; published online June 29, 2017

Abstract: We report on the results of a high-energy x-ray diffraction study of Al–Pd–Mn to investigate the solidification products obtained during free-cooling using an electrostatic levitation furnace. The primary solidification product from the melt is *i*-Al–Pd–Mn which coexists with a significant remaining liquid component. As the sample cools further, we find that the solidification pathway is consistent with the liquidus projection and pseudo-binary cut through the ternary phase diagram reported previously. At ambient temperature we have identified the major phase to be the ξ'-phase orthorhombic approximant, along with minor phases identified as Al and, most likely, the R-phase orthorhombic approximant. We have also observed a distinct prepeak in the liquid at high temperature, signifying the presence of extended atomic order. Interestingly, this prepeak was not observed in previous neutron diffraction measurements on the Al–Pd–Mn system. No undercooling was observed preceding the solidification of the *i*-Al–Pd–Mn phase from the melt which may signal the close similarity of the short-range order in the solid and liquid. However, this can not be clearly determined because of the potential for heterogenous nucleation associated with the presence of an Al_2O_3 impurity at the surface of the sample.

Keywords: electrostatic levitation; high-energy x-ray diffraction; icosahedral phase; phase determination; quasicrystals.

***Corresponding author: Alan I. Goldman,** Department of Physics and Astronomy, Iowa State University, Ames, IA, 50011, USA; and Ames Laboratory, US DOE, Iowa State University, Ames, IA, 50011, USA, E-mail: goldman@ameslab.gov
Dante G. Quirinale, Scott Saunders and Daniel Messina: Department of Physics and Astronomy, Iowa State University, Ames, IA, 50011, USA
Andreas Kreyssig and Paul C. Canfield: Department of Physics and Astronomy, Iowa State University, Ames, IA, 50011, USA; and Ames Laboratory, US DOE, Iowa State University, Ames, IA, 50011, USA
Warren E. Straszheim and Matthew J. Kramer: Ames Laboratory, US DOE, Iowa State University, Ames, IA, 50011, USA

Introduction

Since the discovery of icosahedral quasicrystals [1] by Dan Shechtman 35 years ago, significant effort has been devoted to acquiring a deeper understanding of the conditions for the nucleation and growth of quasicrystalline phases. The Al–Pd–Mn ternary system [2, 3], in particular, has received a great deal of attention because of the relatively high degree of structural perfection demonstrated [4–6] for the icosahedral Al–Pd–Mn phase (*i*-Al–Pd–Mn) near the composition of $Al_{72}Pd_{20}Mn_8$.

The equilibrium ternary phase diagram of this complex intermetallic system is quite rich, and includes several variants of the *i*-phase [7–10], a stable decagonal phase [3, 11] and the close proximity of several related approximant structures [12, 13]. The Al-rich section of the equilibrium ternary phase diagram has been investigated in detail [11–17] and reviewed [18–20] by several groups. Typically, the phase equilibria and solidification pathways were determined through scanning electron microscopy (SEM), transmission electron microscopy (TEM), differential thermal analysis (DTA) and x-ray powder diffraction measurements (XRPD) of annealed and quenched powders or Bridgman-grown single crystals.

Annealing/quenching measurements, of course, assume that the quenched structures reflect the nature of the phases at high temperature, which in many cases is questionable. This is particularly true for complex systems that can be undercooled below the equilibrium solidification temperature to obtain metastable phases [21]. For example, in thermodynamic and x-ray measurements on electrostatically levitated $Ti_{37}Zr_{42}Ni_{21}$, Kelton et al. [22, 23] identified a double recalescence associated with the solidification of an *i*-phase at 1063 K, followed by a second recalescence to the Ti–Zr–Ni Laves phase at 1083 K. Together with their analysis of short-range order (SRO) in the liquid, their results indicate an increase in icosahedral SRO, that is more similar to the *i*-phase than the Laves phase, is associated with deeper undercooling.

In the absence of heterogenous nucleation sites, the extent of undercooling for a particular intermetallic

compound depends largely on the similarity between the local order of the liquid and solid phases; close similarity results in a decrease of the nucleation barrier and, therefore, limits the degree of undercooling that can be realized [24]. This seems to be the case for the quasicrystalline alloys studied to date. For example, Holland-Moritz et al. have performed several undercooling studies of quasicrystal forming alloys of Al–Cu–Fe and Al–Cu–Co [25–27] by electromagnetic levitation (EML), and concluded that the undercoolability of the liquid decreases with the increasing degree of polytetrahedral SRO of the nucleating solid phases. The minimum undercooling was found for the *i*-phase in Al–Cu–Fe and highest for the cubic β-phase in Al–Cu–Co.

More recently, the thermophysical properties of $Al_{72}Pd_{20}Mn_8$ were investigated using electrostatic levitation (ESL) by Ishikawa et al. [28], with the interesting result that no undercooling or distinct recalescence was observed during free-cooling from the melt. This observation led the authors to suggest that clusters, exceeding the critical size, were already present in the liquid. However, two melting plateaus were observed which were attributed to formation of the *i*-phase at 1140 K and orthorhombic approximant phase, ξ', at 1080 K. The ξ' phase is the ternary extension of the γ-Al_3Pd binary phase [15] noted by the authors. However, no direct structural evidence was provided for the identification of the solid phases. In light of the previous work done on the solidification of quasicrystal-forming alloys, we have undertaken a high-energy x-ray diffraction (HEXRD) study of Al–Pd–Mn to investigate the solidification products obtained during free cooling using ESL.

Electrostatic levitation

For investigations of liquids and solids at high temperature, a number of containerless solidification methods [29] have been developed to eliminate the largest source of environmental contamination, the container itself. Concomitantly, non-contact techniques have been developed for the measurement of physical properties such as the liquid density, surface tension, viscosity, specific heat and the liquid structure in equilibrium and nonequilibrium liquids. These techniques are not limited to liquids. They also allow contamination-free studies of structure, phase transitions and thermophysical properties of stable and metastable solids at very high temperatures.

Levitation methods in current use include aerodynamic, ESL and EML. Aerodynamic levitation is achieved by a controlled gas flow through nozzles of optimal design for the size and density of the samples of interest. In principle this method is versatile, enabling studies of metallic, semiconductor or insulating materials. However, the gas flow complicates temperature and positioning control, and can lead to an enhanced heterogeneous nucleation rate. In EML a high frequency magnetic field induces eddy currents within a conducting sample, resulting in a levitation force from the induced magnetic field. Unfortunately, only metallic, or semiconducting materials that become metallic in the liquid phase (e.g. Si, Ge), can be studied. Moreover, since heating and levitation are coupled, the range of accessible undercooling in the levitated state can be quite limited.

In ESL, a positively charged spherical sample is levitated in high vacuum, typically on the order of 10^{-6} Torr, by a dc electric field produced by a pair of vertically spaced electrodes. The sample can then be heated to temperatures in excess of 3000 K using one or more infrared lasers. The sample is initially charged capacitively by contact with the grounded bottom electrode and, once levitated, the sample surface charge is maintained via ultra-violet illumination at low temperatures and by thermionic emission at high temperatures. Two vertical and four horizontal electrodes are used to dynamically stabilize the sample by monitoring the sample position using a fast feedback system to control the voltages. The sample position is maintained by adjusting the control signals provided as input to the dc amplifiers connected to the electrodes, and the position of the levitated sample at the center of the chamber is stable to within ~10 μm. The samples used are spherical with diameters of 1–3 mm. Samples with masses of 20–100 mg can be levitated, however the best processing results have been obtained for sample masses of approximately 30–40 mg.

ESL offers several key advantages over aerodynamic and electromagnetic levitation: (1) non-metallic as well as metallic systems can be studied; (2) the heating and positioning power are decoupled, allowing measurements in more deeply undercooled liquids and; (3) the rf coils required for electromagnetic levitation and the nozzles used in aerodynamic levitation limit the view of the sample, whereas ESL provides a wide range of access to the sample. However, since the processing is accomplished in high vacuum, differences in the vapor pressures of elemental constituents can lead to variations in sample composition during sustained measurements.

High-energy X-ray diffraction (HEXRD)

High energy x-rays from third generation synchrotron sources, such as the Advanced Photon Source, offer clear

benefits for structural studies of ESL-levitated samples. First of all, high-energy x-rays ($E > 100$ keV) suffer much reduced absorption, ensuring that the bulk, rather than the near-surface region, of levitated samples are probed. Since the scattering angles for diffraction vary inversely with the incident beam energy, the range of angles required to capture the full powder pattern using 125 keV x-rays is roughly 15 times smaller than necessary for Cu–Kα radiation. Diffraction patterns can be collected over a wide range of momentum transfer, $Q = 4\pi\sin\theta/\lambda$, for a relatively small range of angles. This, in turn, allows the use of area detectors for fast data acquisition while the sample is either held at a constant temperature or during continuous heating/cooling cycles. The latter method is particularly suitable for continuous studies of phase transformations as the sample is heated from room temperature to the liquidus temperature and above, or radiatively free-cooled from high temperatures.

Experimental details

Single grains of the *i*-Al–Pd–Mn quasicrystal with a composition of $Al_{72(1)}Pd_{20(1)}Mn_{8(1)}$ were grown using the flux-growth [30] algorithm described in previous work [31]. The high-quality samples used in our study were taken from the same batch as those investigated previously by dynamical x-ray diffraction [4]. The quasicrystal was then broken into several smaller pieces, with masses on the order of 30–40 mg, and melted in the Iowa State University ESL (ISU-ESL) [32] on a copper post or graphite block to form ~2 mm spheres for the levitation measurements.

The high-energy x-ray diffraction measurements were performed on beamline 6-ID-D of the Advanced Photon Source (APS) at Argonne National Laboratory using 131 keV x-rays ($\lambda = 0.09441$ Å) and an incident beam cross-section of 0.4×0.4 mm. The samples were electrostatically levitated in the Washington University Beamline Electrostatic Levitator (BESL), a full description of which has been published previously [33]. Two pyrometers were used with complementary temperature ranges to obtain accurate measurements at all temperatures. Above 900 K, the temperature was measured with a Process Sensors Metis MQ22 pyrometer, using two wavelengths to help account for changes in emissivity upon melting. Below 1070 K and above 430 K, a single-color Process Sensors Metis MI18 MB8 was used for lower temperature measurement. The primary source of uncertainty in the temperatures stated in this work arises from changes in sample emissivity with temperature and state. In particular, the emissivity of samples often changes during solidification or solid-solid phase transitions due to electronic changes or the formation of new surface texturing. Indeed, small differences can often be observed in temperature between an undercooled liquid and the ensuing solid. Based upon the temperatures for the transitions measured from many thermal cycles and our experience with these and other similar samples, an error bar of ±10 K is reasonable.

X-ray diffraction patterns were collected using a two-dimensional (2D) Ge Revolution 41-RT flat panel detector. The range of scattering angles accessible in transmission geometry using the 2D detector was $0.9° \le 2\theta \le 19.5°$, allowing measurements over a range of momentum transfers of 1 Å$^{-1} \le Q \le 22.6$ Å^{-1}. Spheres of Si powder mixed with epoxy were levitated as standards to determine detector tilt/rotation and flat-field corrections as well as refining the sample to detector distance to a value of 565 mm, using Fit2D [34, 35]. The diffraction cones appear as rings on the detector which were then azimuthally integrated to obtain a one-dimensional powder pattern. As described in Section "High-energy X-ray diffraction (HEXRD)", the high energy of the x-rays allowed full penetration through the sample, so that the resulting scattering is from the bulk of the 2 mm diameter samples. Diffraction patterns were obtained at frame rates of 1 and 8 fps, however, the data taken at 1 fps are presented here in order to obtain good averaging from textured samples and to represent low-intensity peaks as clearly as possible. Data storage restrictions of the detector system allowed a maximum of 180 frames, providing a maximum data collection time of 180 s at this frame rate.

Once levitated and stable, the samples were slowly brought up above the melt plateau using the diode heating laser ($\lambda = 980$ nm). The samples were overheated by 150–200 K and held for 20–30 s to ensure the samples were fully molten and to facilitate the dissolution of any oxide or impurity phases that were present. Nevertheless, some small translucent patches of aluminum oxide could still be seen on the surface of the levitated molten samples as shown in Figure 1. The presence of stable solid aluminum oxide at the surface is nearly ubiquitous for Al-containing alloys [27, 36] and, of course, raises some concerns regarding the nature of the nucleation mechanism (heterogenous vs. homogeneous) that will be discussed in Section "Discussion". Unfortunately, sustained heating, or heating to much higher temperatures, results in significant mass loss and alters the composition of the sample.

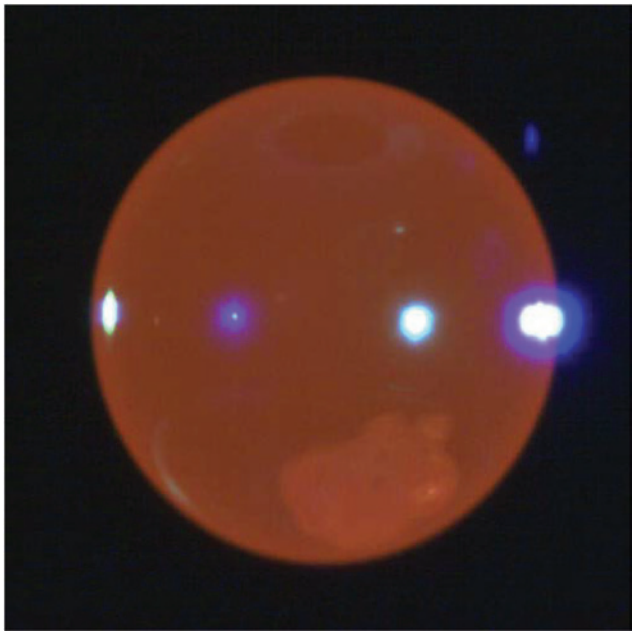

Fig. 1: A view of the liquid sample taken during a heating cycle in the ISU-ESL. The bright spots are reflections of the positioning LEDs. A small translucent patch of Al_2O_3 on the surface of the alloy can be seen in the lower right quadrant of the sphere.

The laser was then shut off and the samples radiatively cooled, and data collected continuously until the limit of the detector memory was reached. Additional scans were taken on heating back up to the liquid. Data were obtained for approximately 20 heating/cooling cycles per sample in order to gain confidence in the phase analysis. The sample was also held in the liquid for 30 s increments to obtain the liquid structure.

Results

High-energy x-ray measurements

A representative free-cooling curve taken during the HEXRD measurements is shown in Figure 2a. During the first 20 s of this measurement the cooling rate is on the order of 20 K/s. At 1130(10) K, we see the first solidification plateau with little, if any, undercooling in evidence. As the temperature decreases further, there is a clear inflection in the cooling curve with a second solidification plateau at 1110(10) K. At lower temperature we observe yet another solidification plateau at ~930(10) K, consistent with the melting point of Al, preceded by approximately 20 K of undercooling. The results here are consistent with the previous measurements of Ishikawa et al. [28], although their data do not extend down below 1000 K.

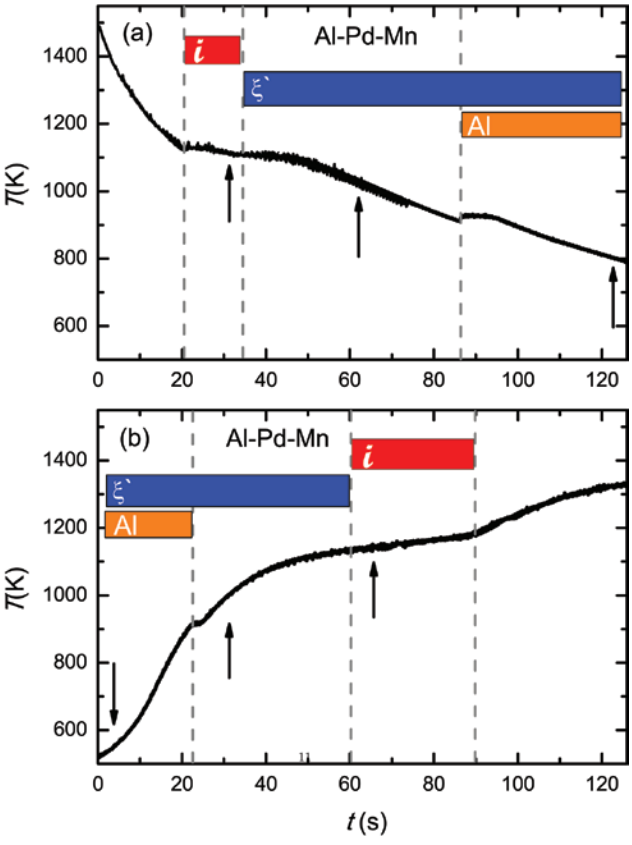

Fig. 2: The (a) cooling and (b) heating curves of the Al–Pd–Mn sample as described in the text. The phases and transition temperatures were identified from the x-ray diffraction patterns and are labeled by the colored bars above the curve. The arrows denote the temperatures for the x-ray diffraction data shown in Figs. 5 and 7.

Figure 3 displays contour plots of the diffraction patterns as a function of temperature on free-cooling from the liquid. Above approximately 1130 K, only the liquid phase is in evidence. Figure 4 shows the liquid structure factor, $S(Q)$ derived from the azimuthally integrated diffraction pattern at 1240 K (~100 K above the first solidification plateau). Two features of $S(Q)$ are notable. First, we see a shoulder on the right side of the second peak in $S(Q)$, at $Q \sim 5.7$ Å^{-1}, that has been observed previously in several quasicrystal-forming systems that manifest icosahedral SRO in the liquid phase [23, 37–42]. Second, a distinct prepeak in $S(Q)$ is found at approximately $Q \sim 2$ Å^{-1}, similar to previous liquid diffraction studies of $Al_{60}Cu_{34}Fe_6$ [43], Al–Co–Ni alloys [42], and liquid Al–Mn alloys [41], and indicative of the presence of extended order in the liquid [44]. In previous studies of Al–Mn, Al–Ni and Al–Cu liquids [41], detailed analysis of the prepeak in $S(Q)$ suggested that it was associated with medium-range order (4–5 Å) involving the transition metal atoms on icosahedral clusters in the liquid. Interestingly, this prepeak was not observed in previous neutron diffraction measurements of the liquid structure in Al–Pd–Mn alloys. One possible explanation is that for neutron measurements, $S(Q)$ is dominated by Al–Al pair contributions, whereas for our x-ray measurements the Al–Pd and Pd–Pd pair correlations contribute substantially. Further measurements that allow a full decomposition of the pair correlations in the liquid phase may shed further light on this issue.

Returning to Figure 2a, we see that the first solid phase to appear on cooling is the *i*-phase of Al–Pd–Mn, which coexists with the liquid over a narrow range in temperature between approximately 1130 K and 1110 K. The corresponding integrated diffraction data are shown in Figures 3 and 5a, displaying the characteristic twin peak structure for the icosahedral phase near $Q = 3$ Å^{-1}. The vertical lines in Figure 5a correspond to the positions and relative intensities of diffraction lines of *i*-Al–Pd–Mn as measured by Tsai et al. [3] at ambient temperature. The smooth green curve in Figure 5(a) represents the raw integrated liquid data used to produce $S(Q)$ in Figure 4 multiplied by a constant factor of 0.95, demonstrating that a substantial fraction of liquid remains in this temperature range.

As the temperature of the sample decreases further, at approximately 1110 K, Figures 3 and 5(b) show that the

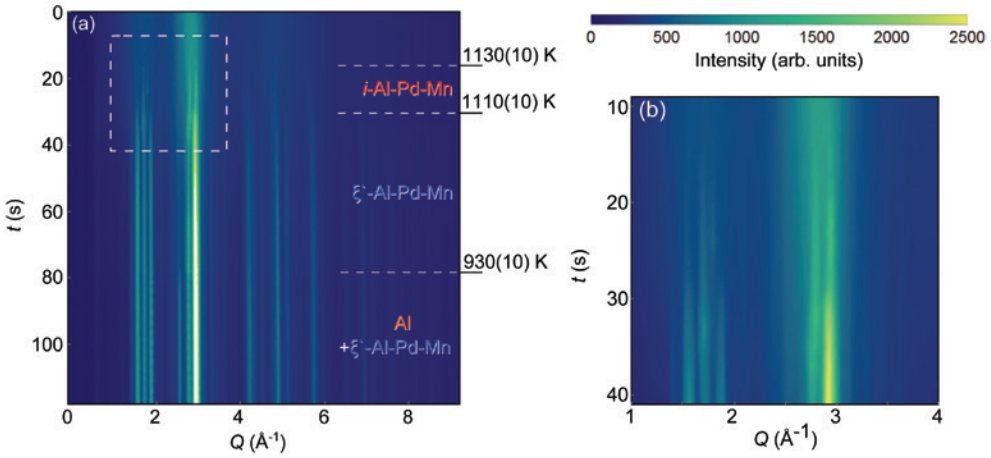

Fig. 3: The azimuthally integrated HEXRD patterns taken on free-cooling the Al–Pd–Mn sample. Panel (a) shows the full temperature/time range of the measurement. The intensity is color-coded. Dashed lines indicate the temperatures at which phases appear in the pattern. Panel (b) displays an expanded view of the temperature and momentum transfer range enclosed by the box in panel (a), where the liquid transforms to the *i*-phase and then to the orthorhombic ξ'-phase.

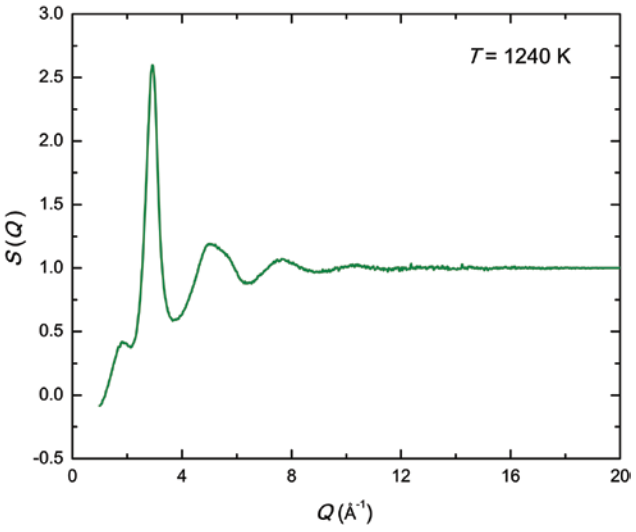

Fig. 4: The liquid structure factor, $S(Q)$, derived from the HEXRD data measured at $T = 1240$ K, which is 100 K above the appearance of the *i*-phase in the sample.

solid and liquid react to form a new solid phase that can be indexed to the orthorhombic ξ' approximant phase, with lattice parameters $a = 23.63(4)$ Å, $b = 16.67(2)$ Å, and $c = 12.27(2)$ Å, in reasonable agreement with previous work [45]. The decrease in the diffuse scattering evident in Figure 5b is consistent with a much smaller fraction of residual liquid in this temperature range.

Upon further cooling, at approximately 930 K, a recalescence event is observed in the temperature profile of Figure 2a, but it is quite difficult to recognize any significant modification of the scattering pattern in Figure 3. A careful comparison between panels (b) and (c) of Figure 5, however, reveals additional intensity at approximately 2.63 Å^{-1}, the position expected for the strongest diffraction peak, Al(111), for face-centered cubic Al. Below this temperature no additional features in the cooling curve, or diffraction patterns were observed.

Figure 2b displays a representative continuous heating curve using a temperature ramp of ~10 K/s. The Al melting plateau at 930(20) K is again clearly observed, as is the full melting of the sample at 1170(20) K. However an intermediate plateau signalling the transition from the dominant ξ' approximant phase to the *i*-phase is not visible. The diffraction data associated with the heating curve in Figure 2b are shown in Figures 6 and 7 which indicate that, on heating, the progression of solid and liquid phases simply reverses with respect to the cooling curve although the plateau temperatures are somewhat higher. At 930(20) K the fcc-Al in the sample melts, at 1130(20) K the dominant ξ' approximant phase decomposes into the *i*-phase and a significant liquid component, and above 1170(20) K, only a liquid diffraction pattern is observed.

Scanning electron microscope (SEM) study

The 2 mm sphere processed in the HEXRD measurement was polished to a depth of ~0.2 mm to reveal a flat face by mechanical polishing and then Ar ion milled. The polished surface was examined using a FEI Teneo SEM at 10 keV while the composition was determined using an Oxford Aztec energy dispersion spectrometer. The average composition, $Al_{69(1)}Pd_{24(1)}Mn_{7(1)}$, was estimated by averaging several energy-dispersive spectra taken at intervals

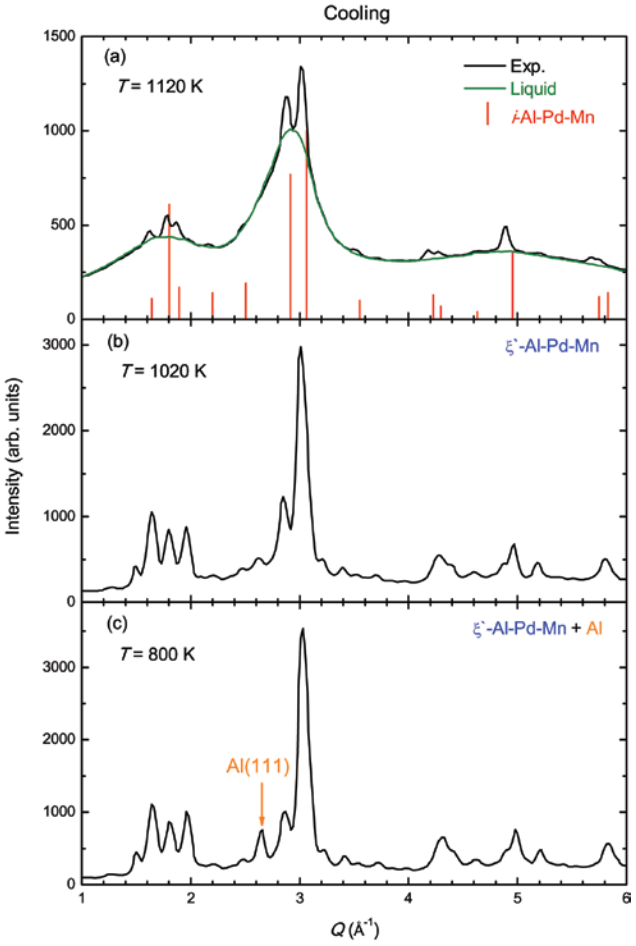

Fig. 5: The azimuthally integrated HEXRD patterns from the Al–Pd–Mn sample during free-cooling at selected temperatures. (a) The pattern at $T = 1120$ K shows the characteristic twin peak pattern from the icosahedral phase. The vertical lines indicate the positions and intensities of the diffraction peaks from published data taken at ambient temperature [3]. The green curve represents the integrated raw liquid data at 1240 K, multiplied by a factor of 0.95. (b) The pattern at $T = 1020$ K is well described by the orthorhombic ξ'-phase [45]. (c) The pattern at $T = 800$ K contains contributions from Al in addition to the primary ξ'-phase.

across a representative region of the sample, and suggests the possibility of some Mn loss due to evaporation during the processing. This is reasonable given the vapor pressure differences between Mn, Al and Pd (10, 10^{-2} and 10^{-4} torr, respectively, at the maximum processing temperature of ~1500 K) [46].

Figure 8 shows a representative backscattered electron image where the dominant light region [phase (a)] is $Al_{70(1)}Pd_{23(1)}Mn_{7(1)}$ (by at.%). The light section is bisected by regions containing two distinctly darker grey regions ranging from a few 10 s to nearly 400 µm. The lighter [phase (b)] is Al intermixed with the primary phase (a), typical of coupled solidification. The regions of much darker contrast [phase (c)] are oxidized Al. It is not clear if the oxidation occurred during sample polishing. The inset shows very small grains with a composition of approximately $Al_{74(1)}Pd_{8(1)}Mn_{17(1)}$ [phase (d)] which are dispersed throughout the matrix. Given the composition of this minor phase and the contours of the liquidus projection of the ternary phase diagram, phase(d) most likely corresponds to the orthorhombic R-phase approximant to i-Al–Pd–Mn [12, 13]. The morphology and the composition of these minor phases suggest that they formed during the latter part of the solidification.

Discussion

The HEXRD together with the chemical and microstructural information paint a coherent picture of the solidification sequence, which is dependent on the initial composition and the cooling rate. The average composition of $Al_{69}Pd_{24}Mn_7$ is near the region in the liquidus projections of the ternary phase diagram [12, 13] close to the ξ' approximant phase. Based on the pseudo-binary cut through the ternary phase diagram [14], the HEXRD data on cooling is consistent with a bulk composition lower in Mn content than the *i*-phase stability region. In this multiphased region, the *i*-phase is stable with respect to the liquid and ξ' phases. During cooling, the initial *i*-phase reacts with the liquid to form ξ' and a residual liquid richer in Al. The residual liquid then forms a eutectic with the ξ' phase and fcc Al. It is unclear if the large aluminum oxide nodules are a result remaining Al liquid which oxidized or unreacted oxides segregated to the intercrystalline regions.

As pointed out in the Introduction, several groups have noted that the degree of undercooling realized for the solidification from the liquid to the *i*-phase is smaller than that for primary solidification to periodic crystalline phases [22, 23, 25–28]. This has been attributed to the presence of icosahedral protoclusters in the liquid so that the SRO in the liquid and solid phases are similar, reducing the nucleation barrier. The presence of icosahedral protoclusters in the liquid phase has also found support from molecular dynamic simulations [47] which found that the growth of the quasicrystalline phase (in this case a decagonal phase) is facilitated by the incorporation of icosahedral protoclusters in close proximity to the nucleation front. In the previous ESL measurements on Al–Pd–Mn samples close in composition to our samples [28], no undercooling was observed. Our measurements find similar results. However, it is well

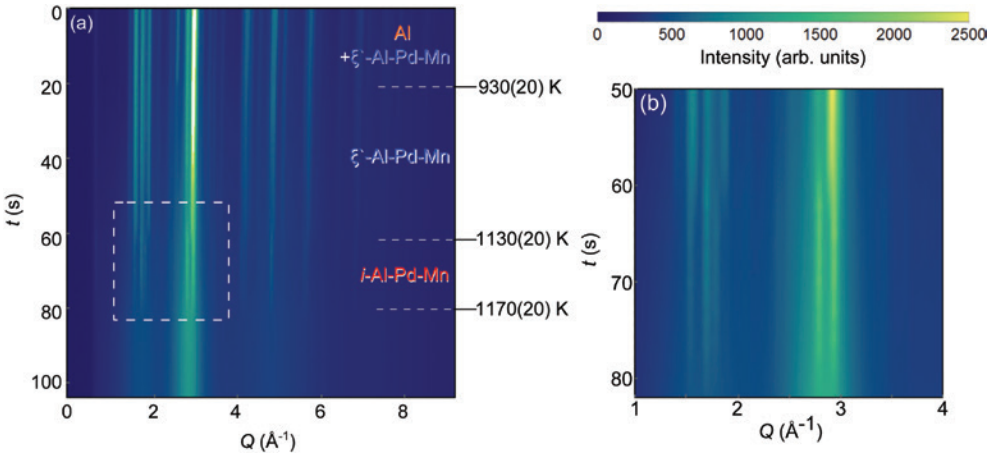

Fig. 6: The azimuthally integrated HEXRD patterns taken on heating the Al–Pd–Mn sample. Panel (a) shows the full temperature/time range of the measurement. Dashed lines indicate the temperatures where phases disappear in the diffraction pattern. Panel (b) displays an expanded view of the temperature and momentum transfer range enclosed by the box in panel (a), where the orthorhombic ξ'-phase transforms to the *i*-phase and then fully melts.

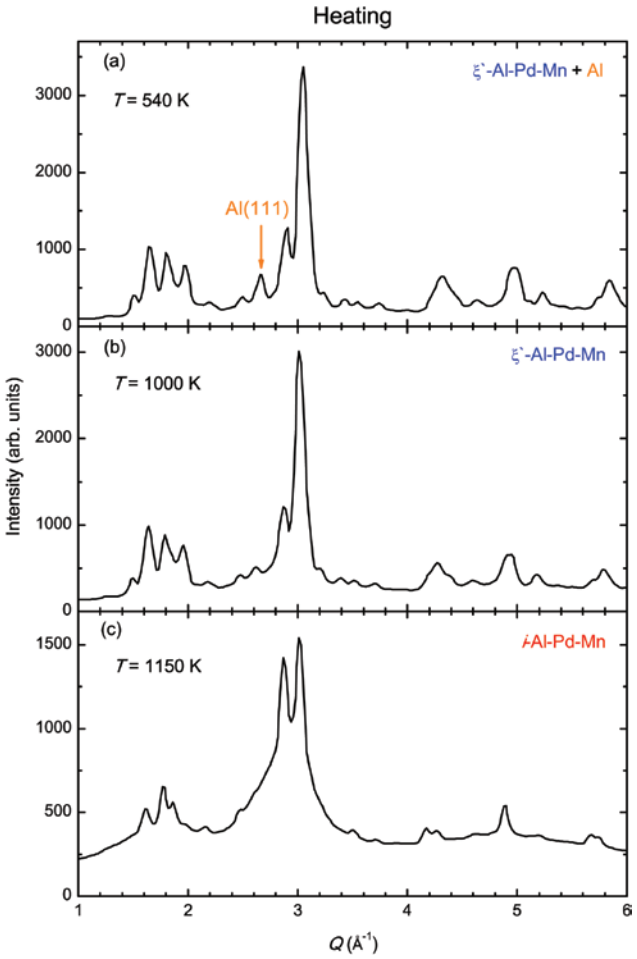

Fig. 7: The azimuthally integrated diffraction patterns from the Al–Pd–Mn sample during heating at selected temperatures. The diffraction pattern at (a) T=540 K and (b) T=1000 K closely reproduce those in the same temperature regimes on free-cooling. (c) The diffraction data at T=1020 K were taken just as the icosahedral phase reappears.

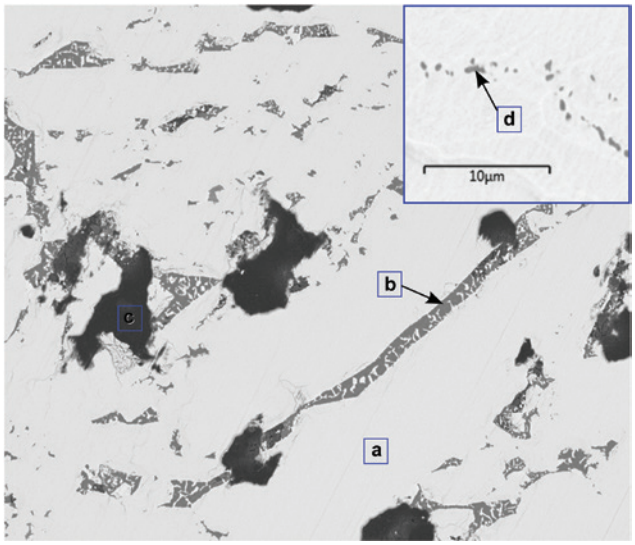

Fig. 8: Backscattered electron image of a section of the ESL-processed Al–Pd–Mn sample. The dominant light regions, labeled (a), correspond to an average composition of $Al_{70}Pd_{23}Mn_7$. The lighter grey region, labeled (b), interspersed with region (a), corresponds to eutectic of Al and the ξ' phase. The darkest regions (c) correspond to oxidized aluminum. The inset is at higher magnification showing a fine distribution of a very fine $Al_{74}Pd_8Mn_{17}$ phase (d).

known that the suppression of undercooling may also arise in the presence of primary heterogenous, rather than homogeneous, nucleation that can occur in the presence of impurity phases (such as Al_2O_3) at the sample surface. This particular impurity is nearly ubiquitous in Al-based alloys and we can not exclude that this is the reason for the absence of any significant undercooling in our measurement.

Summary

Our high-energy x-ray investigation of the solidification products in Al–Pd–Mn close to the ideal composition for the *i*-phase have produced several findings:

- The primary solidification product from the melt is *i*-Al–Pd–Mn and a significant remaining liquid component. The solidification pathway is consistent with the liquidus projection [12, 13] and pseudo-binary cut through the ternary phase diagram [14]. No additional high-temperature stable or metastable phases were observed.
- For the average composition of $Al_{69}Pd_{24}Mn_7$, further cooling results in the formation of the ξ' orthorhombic approximant as the major phase at ambient temperature, along with minor phases identified as Al and, most likely, the R-phase orthorhombic approximant. Upon reheating, the solidification path reverses.
- We have observed a distinct prepeak in the liquid at high temperature, signifying the presence of extended atomic order. This prepeak was not observed in previous neutron diffraction measurements on the Al–Pd–Mn system [38, 39], and may possibly arise from the Al–Pd and or Pd–Pd pair correlations in the liquid which x-rays probe more sensitively.
- No undercooling was observed preceding the solidification of the *i*-Al–Pd–Mn phase from the melt which may signal the close similarity of the SRO in the solid and liquid. However, this can not be clearly determined because of the potential for heterogenous nucleation associated with the Al_2O_3 impurity phase at the surface of the sample.

The HEXRD work at the Advanced Photon Source was supported by the National Science Foundation under Grant No. DMR-1308099. The work at Ames Laboratory was supported by the U.S. Department of Energy, Basic Energy Sciences, of Materials Science and Engineering Division, under Contract No. DE-AC02-07CH11358. The APS is operated by Argonne National Laboratory under the U.S. DOE Contract DE-AC02-06CH11357. The authors would like to acknowledge the assistance of R. Ashcroft, C. Pueblo, K. F. Kelton and D. S. Robinson with the HEXRD measurements and T. Lograsso for enlightening discussions.

References

[1] D. Shechtman, I Blech, D. Gratias, J. W. Cahn, *Phys. Rev. Lett.* **1984**, *53*, 1951.
[2] A. P. Tsai, A. Inoue, Y. Yokoyama, T. Masumoto, *Phil. Mag. Lett.* **1990**, *61*, 9.
[3] A. P. Tsai, A. Inoue, Y. Yokoyama, T. Masumoto, *Mater. Trans. JIM* **1990**, *31*, 98.
[4] S. Kycia, A. I. Goldman, T. A. Lograsso, D. W. Delaney, D. Black, M. Sutton, E. Dufresne, R. Brüning, B. Rodricks, *Phys. Rev. B* **1993**, *48*, 3544.
[5] Y. Zhang, *Ph.D. Thesis*, Purdue University, West Lafayette, **1997**.
[6] J. Härtwig, S. Agliozzo, J. Baruchel, R. Colella, M. de Boissieu, J. Gastaldi, H. Klein, L. Mancini, J. Wang, *J. Phys. D: Appl. Phys.* **2001**, *34*, A103.
[7] T. Ishimasa, M. Mori, *Phil. Mag. B* **1992**, *56*, 513.
[8] M. de Boissieu, M. Boudard, T. Ishimasa, E. Elkaim, J. P. Lauriat, A. Letoublon, M. Audier, M. Duneau, A. Davroski, *Phil. Mag. A* **1998**, *78*, 305.
[9] I. Hirai, T. Ishimasa, A. Letoublon, M. Boudard, M. de Boissieu, *Mater. Sci. Eng. A*, **2000**, *33*, 294.
[10] A. Letoublon, T. Ishimasa, M. de Boissieu, M. Boudard, B. Hennion, M. Mori, *Phil. Mag. Lett.* **2000**, *80*, 205.
[11] C. Beeli, H. -U. Nissen, J. Robadey, *Phil. Mag. Lett.* **1990**, *63*, 87.
[12] M. Audier, M. Durand-Charre, M. de Boissieu, *Phil. Mag. B* **1993**, *68*, 607.
[13] H. Klein, M. Durand-Charre, M. Audier, *J. Alloys Compd*. **2000**, *296*, 128.
[14] Y. Yokoyama, A. -P. Tsai, A. Inoue, T. Masumoto, *Mater. Trans. JIM* **1991**, *32*, 1089.
[15] B. Grushko, M. Yurechko, N. Tamura, *J. Alloys Compd*. **1999**, *290*, 164.
[16] T. Godecke, R. Luck, *Z. Metallkd*. **1995**, *86*, 109.
[17] S. Balanetskyy, G. Meisterernst, M. Heggen, M. Feuerbacher, *Intermetallics* **2008**, *16*, 71.
[18] O. Dovbenko, T. Velikanova, S. Balanetskyy, Aluminum-Manganese-Palladium. in *Ternary Alloy Systems. Phase Diagrams, Crystallographic and Thermodynamic Data Critically Evaluated by MSIT. Group IV: Physical Chemistry. Subvolume A – Light Metal Systems* (Ed. G. Effenberg), Springer, New York, **2005**.
[19] V. Raghavan, *J. Phase Equilib. Diffus.* **2008**, *29*, 63.
[20] V. Raghavan, *J. Phase Equilib. Diffus.* **2009**, *30*, 71.
[21] D. Herlach, P. Galenko, D. Holland-Moritz, *Metastable Solids from Undercooled Melts*, Pergamon, Oxford, **2007**.
[22] K. F. Kelton, A. K. Gangopadhyay, G. W. Lee, L. Hannet, R. W. Hyers, S. Krishnan, M. B. Robinson, J. Rogers, T. J. Rathz, *J. Non-cryst. Solids* **2002**, *312–314*, 305.
[23] K. F. Kelton, G. W. Lee, A. K. Gangopadhyay, R. W. Hyers, T. J. Rathz, J. R. Rogers, M. B. Robinson, D. S. Robinson, *Phys. Rev. Lett.* **2003**, *90*, 195504.
[24] D. R. Nelson, F. Spaepen, Polytetrahedral order in condensed matter. in *Solid State Physics 42* (Eds. H. Ehrenreich, D. Turnbull), Academic Press, New York, **1989**.
[25] D. Holland-Moritz, D. M. Herlach, K. Urban, *Phys. Rev. Lett.* **1993**, *71*, 1196.
[26] D. Holland-Moritz, D. M. Herlach, B. Grushko, K. Urban, *Mater. Sci. Eng*. **1994**, *A181/A182*, 766.
[27] D. Holland-Moritz, J. Schroers, D. M. Herlach, B. Grushko, K. Urban, *Acta Mater.* **1998**, *46*, 1601.
[28] R. Ishikawa, T. Ishikawa, J. T. Okada, T. Maski, Y. Watanabe, S. Nanao, *Phil. Mag*. **2007**, *87*, 2965.
[29] D. L. Price, *High-temperature Levitated Materials*, Cambridge, New York **2010**, and references therein.
[30] P. C. Canfield, Z. Fisk, *Phil. Mag. B* **1992**, *65*, 1117.

[31] I. R. Fisher, M. J. Kramer, T. A. Wiener, Z. Islam, A. R. Ross, T. A. Lograsso, A. Kracher, A. I. Goldman, P. C. Canfield, *Phil. Mag. B* **1999**, *79*, 1673.
[32] G. E. Rustan, N. S. Spyrison, A. Kreyssig, R. Prozorov, A. I. Goldman, *Rev. Sci. Instrum.* **2012**, *83*, 103907.
[33] N. A. Mauro, K. F. Kelton, *Rev. Sci. Instrum.* **2011**, *82*, 035114.
[34] A. P. Hammersley, S. O. Svensson, M. Hanfland, A. N. Fitch, D. Häusermann, *High Press. Res.* **1996**, *14*, 235.
[35] A. P. Hammersley, ESRF Internal Report ESRF97HA02T, **1997**.
[36] G. E. Rustan, *Ph.D. Thesis*, Iowa State University, Ames, **2014**.
[37] S. Sachdev, D. R. Nelson, *Phys. Rev. Lett.* **1984**, *53*, 1947.
[38] V. Simonet, F. Hippert, H. Klein, M. Audier, R. Bellissent, H. Fischer, A. P. Murani, D. Boursier, *Phys. Rev. B* **1998**, *58*, 6273.
[39] V. Simonet, F. Hippert, M. Audier, R. Bellissent, *Phys. Rev. B* **2001**, *65*, 024203.
[40] D. Holland-Moritz, T. Schenk, V. Simonet, R. Bellisent, P. Convert, T. Hansen, D. M. Herlach, *Mater. Sci. Eng. A* **2004**, *375–377*, 98.
[41] A. S. Roik, S. N. Galushko, A. V. Samsonnikov, V. P. Kazimirov, V. E. Sokol'skii,V. A. Shovskii, *Metally* **2009**, *2009*, 201.
[42] O. S. Roik, O. Samsonnikov, V. Kazimirov, V. Sokolskii, *Z. Naturforsch.* **2010**, *65a*, 123.
[43] D. Holland-Moritz, T. Schenk, V. Simonet, R. Bellisent, *Phil. Mag.* **2006**, *86*, 255.
[44] L. Wang, H. G. Cong, Y. I. Zhang, X. F. Bian, *Physica B* **2005**, *355*, 140.
[45] M. Boudard, H. Klein, M. de Boissieu, M. Audier, H. Vincent, *Phil. Mag. A* **1996**, *74*, 939.
[46] R.E. Honig, D. A. Kramer, *Vapor Pressure Curves of the Elements*, RCA Laboratories, Princeton, **1966**.
[47] A. S. Keys, S. C. Glotzer, *Phys. Rev. Lett.* **2007**, *99*, 235503.